Article

Development of Glass-Ceramics Containing Possible NASICON-Type Phases Derived from Soda-Lime Glass Waste, Zirconia Residue, and Bentonite

Edson de Oliveira Costa *, Maria Aparecida Ribeiro Bonifácio , Adriana de Jesus Santos , Cochian Pereira dos Santos , José Carlos Martins de Almeida , Eliane Bezerra Cavalcanti , Valdenia Porto Medeiros , Crislene Rodrigues da Silva Morais

Posted Date: 19 May 2026

doi: 10.20944/preprints202605.1253.v1

Keywords: glass-ceramic foams; industrial waste recycling; NASICON structure

 doi:10.20944/preprints202605.1253.v1

Article

Development of Glass-Ceramics Containing Possible NASICON-Type Phases Derived from Soda-Lime Glass Waste, Zirconia Residue, and Bentonite

Edson de Oliveira Costa [1,*], Maria Aparecida Ribeiro Bonifácio [2], Adriana de Jesus Santos [3], Cochian Pereira dos Santos [4], José Carlos Martins de Almeida [5], Eliane Bezerra Cavalcanti [3], Valdenia Porto Medeiros [6] and Crislene Rodrigues da Silva Morais [1,2]

[1] Graduate Program in Materials Science and Engineering (PPG-CEMat), Federal University of Campina Grande, Av. Aprígio Veloso-882, Bodocongó, Campina Grande 58429-900, PB, Brazil
[2] Academic Unit of Materials Engineering, Science and Technology Center, Federal University of Campina Grande, Av. Aprígio Veloso-882, Bodocongó, Campina Grande 58429-900, PB, Brazil
[3] Institute of Technology and Research (ITP), Tiradentes University, Aracaju, SE, Brazil
[4] Physics Department, Federal University of Sergipe, São Cristóvão, SE, Brazil
[5] Department of Materials and Ceramic Engineering and CICECO – Aveiro Institute of Materials, University of Aveiro, Aveiro, Portugal
[6] Federal Institute of Education, Science and Technology of Paraíba (IFPB), João Pessoa Campus, Av. Primeiro de maio, 720, Jaguaribe, João Pessoa, PB 58015-430, Brazil
* Correspondence: edson.oliveira@estudante.ufcg.edu.br

Abstract

Glass-ceramic foams (BVZ: bottle glass waste–zirconia residue–bentonite) were produced using the polymeric replica method from low-cost raw materials, comprising approximately 85 wt% bottle glass waste and zirconia residue, and 15 wt% regional bentonite. To evaluate the effect of zirconia residue on the microstructure and physicochemical properties of the BVZ foams, aqueous precursor suspensions were prepared with varying proportions of bottle glass waste (59.7–69.7 wt%) and zirconia residue (14.9–19.9 wt%), and sintered at 750 °C, 800 °C, and 850 °C. X-ray diffraction (XRD) analysis revealed a reduction of the amorphous halo (15–35° 2θ) and an increase in crystallinity with increasing temperature, indicating devitrification of the glassy matrix. The main crystalline phases identified were zircon ($ZrSiO_4$), nepheline ($NaAlSiO_4$), $AlPO_4$, and zirconia (ZrO_2), with evidence of minor domains structurally compatible with NASICON-type phases ($NaZr_2(PO_4)_3$). In general, glass-ceramic foams produced with high waste content showed greater densification and reduced porosity at 850 °C. The mechanical strength was sufficient for handling and assembly in electrochemical cell components, while the reduced brittleness supports safe processing and indicates potential for scalable manufacturing.

Keywords: glass-ceramic foams; industrial waste recycling; NASICON structure

1. Introduction

The development of sustainable materials based on the recycling of industrial by- products has received increasing attention in functional materials, particularly to produce porous glass-ceramics, due to their multifunctional properties and potential for structural and environmental applications [1,2].

Among alternative raw materials, glass waste has been widely investigated for the fabrication of glass-ceramics, which exhibit low density, high mechanical strength, low thermal conductivity, incombustibility, and chemical resistance. These characteristics make such materials suitable for

 doi:10.20944/preprints202605.1253.v1

applications in the construction industry, particularly as thermal and acoustic insulating materials [3–5].

Powder sintering is traditionally one of the main processing routes for producing glass-ceramics, in which glass powders are subjected to controlled heat treatments to promote crystallization of the glassy matrix [6]. During sintering, the glass softens, and the foaming agents employed release gases, leading to bubble formation within the viscous matrix. As temperature increases, the reduction in glass viscosity and surface tension favors bubble expansion and the development of porosity [3,7,8]. Conventional foaming agents include carbonates, sulfates, silicates, and carbon-based materials, which decompose upon heating and release gaseous species.

However, alternative routes for producing porous glass-ceramics have also been explored, such as gel casting, freeze casting, pore-forming agent-assisted methods, and the polymeric sponge technique, also known as the replica method [9,10]. In this approach, porosity is generated through the thermal decomposition of a sacrificial polymer template previously impregnated with a glass suspension [2]. This method enables improved control over pore architecture and pore interconnectivity and is particularly promising for obtaining lightweight structures with high specific surface area.

Despite advances in sustainable glass-ceramic materials, the combined use of different residues in the development of NASICON-type porous systems remains limited, especially regarding phase evolution and the resulting microstructure under different thermal treatment conditions.

Therefore, the present study aimed to develop NASICON-type porous glass-ceramics using soda-lime glass waste, zirconia residue, and bentonite through the polymeric replica method. The study investigates structural evolution, crystalline phase formation, and the influence of thermal treatment conditions on the properties of the resulting foams.

2. Materials and Methods

2.1. Synthesis of Glass-Ceramics

The replica method was employed to produce glass-ceramics from bentonite, glass waste, and zirconia residue investigated in this study. Open-cell polyurethane foams with a pore density of 25 ppi were used as templates. The raw materials consisted of soda-lime glass bottle waste, zirconia residue, bentonite (used as a plasticizer), and sodium silicate (used as a dispersant). The chemical composition was determined by energy-dispersive X-ray spectroscopy (EDX) using a SHIMADZU EDX-720 system to define the slip formulations.

The soda–lime glass waste was crushed and milled in a ball mill (Servitech, CT-242) at 380 rpm for 30 minutes. The raw materials were sieved through an ABNT Nº. 200 mesh (74 μm), and the average particle size was determined by dynamic light scattering (DLS) using an SZ-100 nanoparticle analyzer (HORIBA Scientific). The crystalline phases present in the raw materials were identified by X-ray diffraction (XRD) using a Bruker D2-Phaser diffractometer equipped with Cu Kα radiation (λ = 1.5418 Å). Measurements were carried out over a 2θ range of 5°-80°, with a step size of 0.02°.

Three suspensions (BVZs) were prepared according to compositions reported in previous studies, which emphasize the importance of balancing rheological properties and sinterability to obtain glass-ceramics with optimized functional performance [1,2]. The formulation of the precursor slips for the glass-ceramics are presented in Table 1. The three suspensions were designated BVZ1, BVZ2, and BVZ3.

Table 1. Formulations of aqueous precursor suspensions used to produce BVZ glass-ceramics.

Glass ceramics	Composition (%wt.)		Solid content (%wt)			
	Solid content	Liquid content	Bentonite	Glass Waste	Zirconia Waste	Sodium Silicate
BVZ1	74.2	25.8	14.9	69.7	14.9	0.5
BVZ2	70.6	29.4	14.8	64.8	19.9	0.5

 doi:10.20944/preprints202605.1253.v1

BVZ3	70.7	29.3	19.9	59.7	19.9	0.5

The raw materials were homogenized in a mechanical mixer at 600 rpm for 30 minutes. The polyurethane foams were subsequently immersed in the prepared suspension at 30-minute intervals. After impregnation, the foams were calendered to remove excess slurry. The drying process was carried out in two stages: first at room temperature for 24 hours, followed by oven drying at 110 °C for 2 hours. Finally, the impregnated foams were subjected to heat treatment at different temperatures to obtain the glass-ceramics, as illustrated in Figure 1 [1,3].

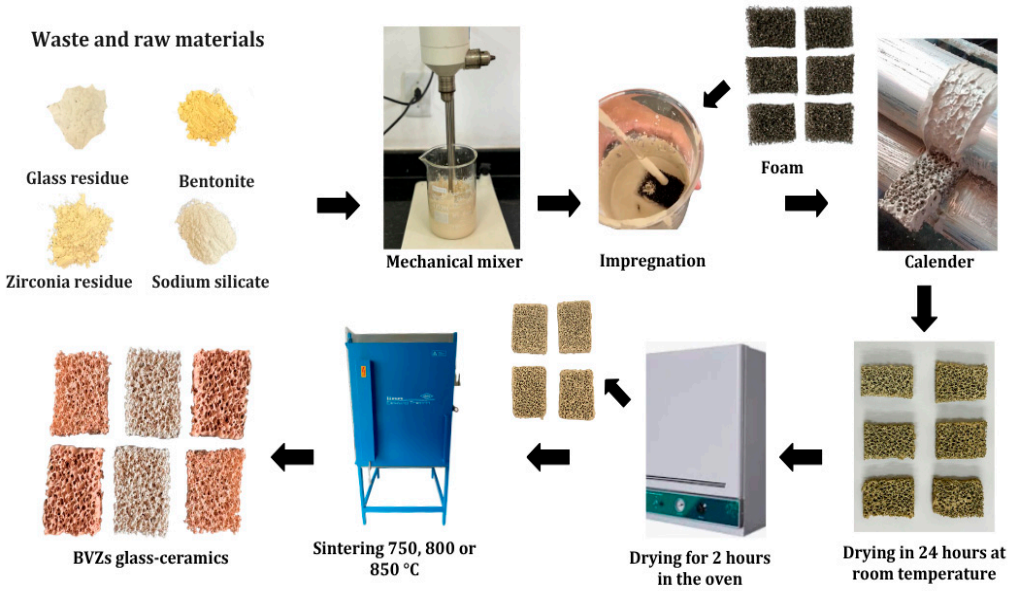

Figure 1. Synthesis process of glass-ceramics.

The sintering process was carried out at 750 °C, 800 °C, and 850 °C for 60 minutes. The cooling procedure was performed in three stages: first, the samples were cooled to 540 °C and held for 30 minutes, then cooled to 440 °C and held for 60 minutes. In both stages, a cooling rate of 10 °C·min^{-1} was applied. Finally, the samples were cooled to room temperature by the natural thermal inertia of the furnace, as shown in Figure 2. A progressive lightening in color can be observed with increasing sintering temperature. However, the BVZ3 glass-ceramic exhibits a darker coloration due to the higher Fe_2O_3 content originating from the bentonite.

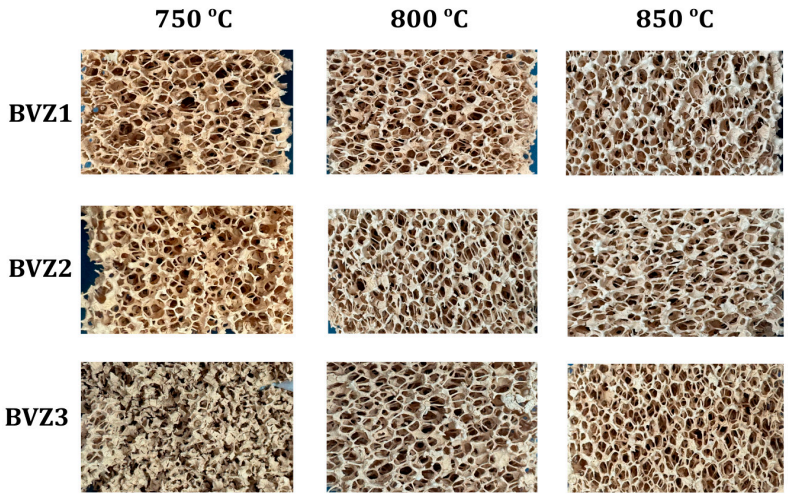

 doi:10.20944/preprints202605.1253.v1

Figure 2. Images acquired of glass-ceramic foams BVZ1, BVZ2 E BVZ3 obtained at temperatures of 750 °C, 800 °C and 850 °C.

2.2. Characterization of the Glass-Ceramics

The chemical composition of the raw materials, in terms of the oxides present, was determined by energy-dispersive X-ray spectroscopy (EDX) using a SHIMADZU EDX-720 system. The amorphous/crystalline nature of the glass-ceramics was characterized by X-ray diffraction (XRD) using an X'Pert Pro³ diffractometer (PANalytical, Netherlands) equipped with a Cu Kα radiation source. Measurements were performed over a 2θ range of 10°-130°, with a step size of 0.02°. Optical photomicrographs were acquired using an OPTIKA SLX stereomicroscope.

The glass transition temperature (Tg), crystallization onset temperature (Tc), and crystallization peak temperature (Tp) were determined by differential thermal analysis (DTA) using a SHIMADZU DTG-60H thermal analyzer. The experiments were conducted under a nitrogen atmosphere with a flow rate of 50 mL·min^{-1}, a heating rate of 10 °C·min^{-1}, and alumina crucibles. The accuracy of the characteristic temperature measurements was ±1.5 °C.

The mechanical strength of the glass-ceramic foams was evaluated by compression testing using a universal testing machine (SHIMADZU AG-25TA, Trapezium) equipped with a 1 kN load cell, at a crosshead speed of 0.5 mm·min^{-1}.

3. Results

3.1. Characterization of Raw Materials

3.1.1. EDX Analysis of the Chemical Composition of Raw Materials

Table 2 presents the chemical composition of the raw materials. The glass waste used in this study is classified as soda-lime-silica glass, as evidenced by the high contents of SiO_2 (70.3 wt%), Na_2O (12.3 wt%), and CaO (12.0 wt%). In addition, the presence of Al_2O_3 (4.1 wt%) contributes to increased mechanical strength and thermal stability of the glassy matrix, as widely reported in the literature [1,2]. The zirconia residue exhibits a markedly different chemical profile, with a high P_2O_5 content (41.9 wt%), followed by significant amounts of ZrO_2 (34.5 wt%) and SiO_2 (21.3 wt%).

The high concentration of ZrO_2 suggests strong potential for improving the mechanical and thermal properties of the resulting glass-ceramic system, while the presence of P_2O_5 may influence crystallization behavior and phase formation during heat treatment [11]. The bentonite originating from northeastern Brazil [12] showed SiO_2 (56.0 wt%) and Al_2O_3 (30.6 wt%) as the predominant oxides, followed by Fe_2O_3 (5.3 wt%). The presence of Na_2O, MgO, and CaO confirms its polycationic nature and its influence on viscosity, sintering behavior, and pore formation in the glass-ceramics.

Table 2. Chemical composition of the raw materials.

Raw Materials	Composição (wt%)											
	SiO_2	Na_2O	CaO	Al_2O_3	K_2O	SO_3	Fe_2O_3	TiO_2	MgO	ZrO_2	HfO_2	P_2O_5
Glass-Waste	70.3	12.3	12.0	4.1	0.6	0.4	0.2	0.1	---	---	---	---
Zirconia Waste	21.3	---	---	1.5	---	---	0.1	---	---	34.5	0.5	41.9
Bentonite	56.0	2.4	1.1	30.6	---	0.5	5.3	0.7	2.0	---	---	---

3.1.2. Granulometric Compatibility of Raw Materials

The particle size characterizations (Table 3 and Figure 3) reveal that zirconia (Dm = 0.186 μm), bentonite (Dm = 0.121 μm), and glass (Dm = 0.113 μm) exhibit a strictly submicrometric nature (D90

 doi:10.20944/preprints202605.1253.v1

< 1 μm) and narrow monomodal distributions. This high degree of uniformity enhances chemical reactivity and microstructural control, reducing defects in the final product [13–15]. In particular, the dimensional similarity between glass and bentonite is strategically important for processing; according to [15,16], this granulometric synergy optimizes the dispersion of the glassy phase within the ceramic matrix. This condition promotes the formation of a homogeneously distributed liquid phase during heat treatment, resulting in superior structural consolidation of the glass-ceramics.

Table 3. Granulometric distribution of raw materials.

Raw 2.	Fine (x < 2 μm)	D_{10} (μm)	D_{50} (μm)	D_{90} (μm)	Dm (μm)
Zirconia Waste	100%	0.140	0.181	0.260	0.186
Bentonite	100%	0.105	0.115	0.140	0.121
Glass Waste	100%	0.085	0.100	0.160	0.113

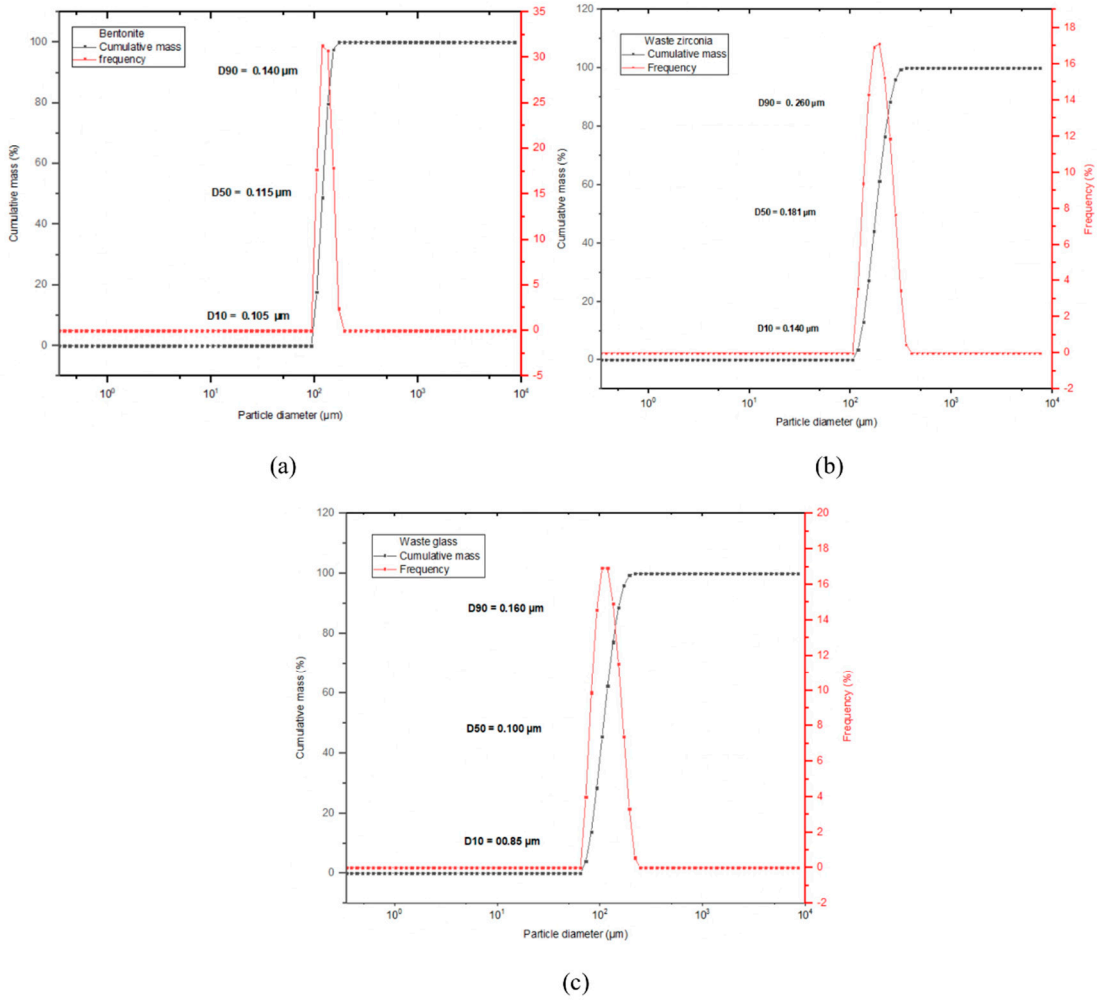

Figure 3. Granulometric distribution of the waste glass (**a**), waste zirconia (**b**) and bentonite (**c**).

3.1.3. XRD Analysis of Raw Materials

Figure 4 presents the diffraction patterns of the glass waste (a), zirconia residue (b), and bentonite (c), respectively. The X-ray diffraction pattern of the soda–lime glass waste (Figure 4a) is characterized by a diffuse halo between approximately 20° and 30° (2θ), typical of amorphous materials, confirming the glassy nature of the silicate matrix. The absence of sharp, well-defined peaks indicates that no crystalline phases are detectable within the limits of the technique,

 doi:10.20944/preprints202605.1253.v1

demonstrating that the material is predominantly amorphous, in agreement with the expected behavior of soda–lime glass waste [17].

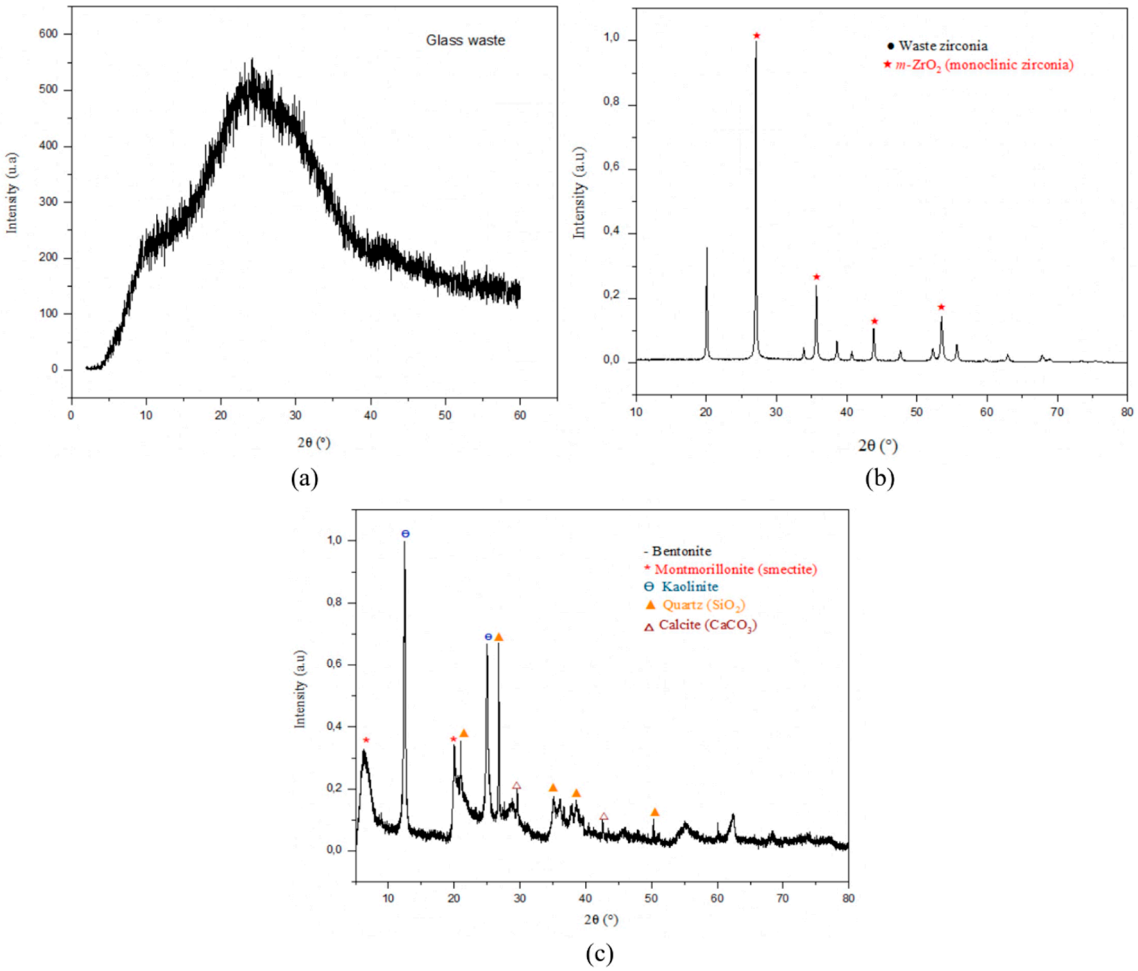

Figure 4. X-ray diffraction patterns of (**a**) glass waste, (**b**) zirconia residue, and (**c**) bentonite.

The X-ray diffraction (XRD) pattern of the zirconia residue (Figure 4b) reveals the predominant presence of the monoclinic ZrO_2 phase, characterized by intense reflections at $2\theta \approx 28.2°$ and 34.3°, along with secondary peaks at higher angles, confirming the dominance of this crystalline phase [18,19]. The presence of sharp and well-defined peaks indicates a high degree of crystallinity of the m-ZrO_2 phase. A diffuse halo around $2\theta \approx 20°$ is also observed, associated with an amorphous fraction, a feature frequently found in industrial residues and zirconia particulate materials [19]. No reflections related to tetragonal or cubic phases were observed, indicating the absence of dopant-induced stabilization.

The X-ray diffraction (XRD) pattern of bentonite (Figure 4c) shows a mineralogical composition typical of bentonitic clays, with a basal reflection at low angles ($2\theta \approx 5–7°$) associated with montmorillonite, the main phase responsible for the technological properties of bentonite, such as high cation exchange capacity, swelling behavior, and rheological characteristics [20,21]. Additional peaks around $2\theta \approx 12.3°$ and 24.8° indicate the presence of kaolinite, while the intense reflection at ≈ 26.6° is attributed to quartz (SiO_2), a common accessory mineral in natural bentonites. Low-intensity reflections at higher angles, including signals consistent with calcite ($CaCO_3$), indicate the presence of carbonate phases in trace amounts, in agreement with quantitative XRD analyses reported in the literature [22].

 doi:10.20944/preprints202605.1253.v1

3.2. Characterization of Glass-Ceramics

3.2.1. Chemical Composition and Role of Oxides in the Sintering of BVZ Glass-Ceramics

The compositions of the BVZ glass-ceramics (Table 4) characterize a complex silicate system with a high zirconia content (17.4-22.0 wt%), which acts as the main reinforcing refractory phase. Silica (SiO_2) is the predominant network former (44.9-51.0 wt%), while the low alumina content (3.2-3.9 wt%) prevents the system from being classified as an aluminosilicate. Structural integrity arises from the network modified by fluxing oxides (Na_2O and CaO, 15-18 wt%), which promote sintering through liquid-phase formation. Phosphorus pentoxide (P_2O_5) acts as a nucleating agent (6.2-10.5 wt%), while iron oxide (Fe_2O_3) is present as a minor constituent (0.6-2.1 wt%). At 850 °C, this compositional profile promotes atomic diffusion and the encapsulation of zirconia within a dense glassy matrix, as discussed by [23].

Table 4. Chemical composition of BVZs glass-ceramics.

Glas-Ceramics	Composition (wt%)										
	SiO_2	Na_2O	CaO	Al_2O_3	K_2O	ZrO_2	Fe_2O_3	TiO_2	MgO	HfO_2	P_2O_5
BVZ1	51.0	9.0	9.4	3.4	0.7	17.4	1.7	0.3	0.4	0.3	6.2
BVZ2	45.8	7.5	8.3	3.2	0.6	22.0	1.6	0.3	0.4	0.4	9.6
BVZ3	44.9	7.1	7.7	3.9	0.6	21.7	2.1	0.4	0.5	0.4	10.5

3.2.2. Phase Evolution and Structural Characterization by X-Ray Diffraction (XRD)

The X-ray diffraction patterns of the BVZ samples (Figures 5, 6, and 7), sintered at 750 °C, 800 °C, and 850 °C, exhibit behavior typical of glass-ceramic materials obtained through controlled heat treatment. In all compositions, the simultaneous presence of an amorphous halo centered in the 15-35° (2θ) range and crystalline diffraction peaks is observed, confirming the coexistence of a residual glassy phase and crystalline phases formed during sintering [24]. With increasing temperature, a progressive reduction in the amorphous contribution and an increase in the intensity and sharpness of the crystalline peaks are evident, indicating the advancement of the devitrification process and the growth of crystalline domains [25,26].

This behavior is characteristic of glass-ceramics, in which the structural reorganization of the glassy matrix promotes the nucleation and growth of thermodynamically more stable crystalline phases. The identification of crystalline phases was performed by comparison with crystallographic standards available in the Crystallography Open Database (COD), using the Match! software for phase analysis.

Figure 5 shows the evolution of crystalline phases in the BVZ1 sample with increasing sintering temperature. At 750 °C, the most intense peaks are consistent with nepheline ($NaAlSiO_4$, COD 96-901-3314) and $AlPO_4$ (COD 96-155-0017), along with reflections attributed to zircon ($ZrSiO_4$, COD 96-900-2563) and cristobalite (SiO_2, COD 96-901-5301). The presence of these phases indicates that, at this temperature, crystallization is predominantly governed by the structural reorganization of silicate and aluminosilicate phases derived from soda–lime glass and bentonite.

 doi:10.20944/preprints202605.1253.v1

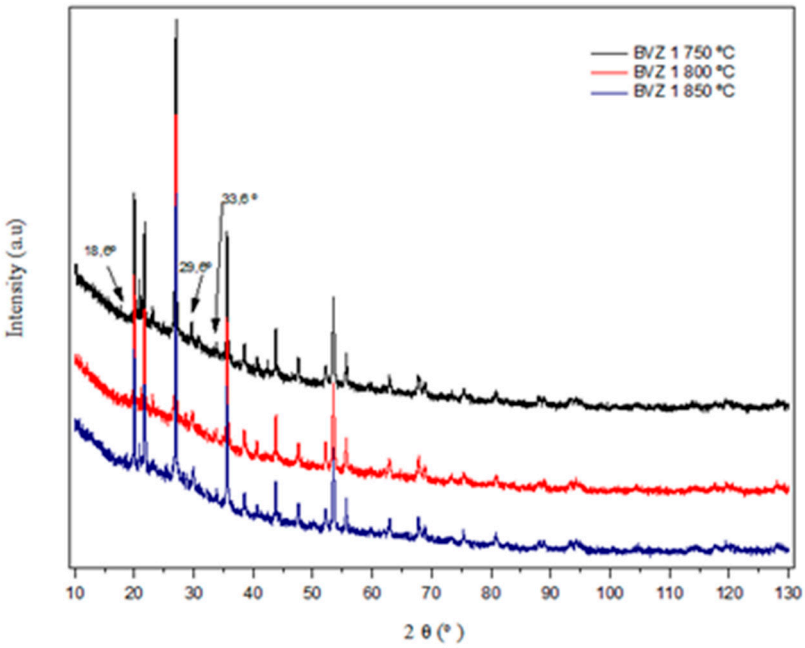

Figure 5. X-ray diffraction (XRD) patterns of BVZ1 glass-ceramics sintered at 750 °C, 800 °C, and 850 °C, showing the evolution of crystalline phases with increasing temperature.

Figure 6 reveals significant changes in the evolution of crystalline phases in the BVZ2 sample compared to BVZ1, particularly regarding the role of zirconium- and phosphate-containing phases.

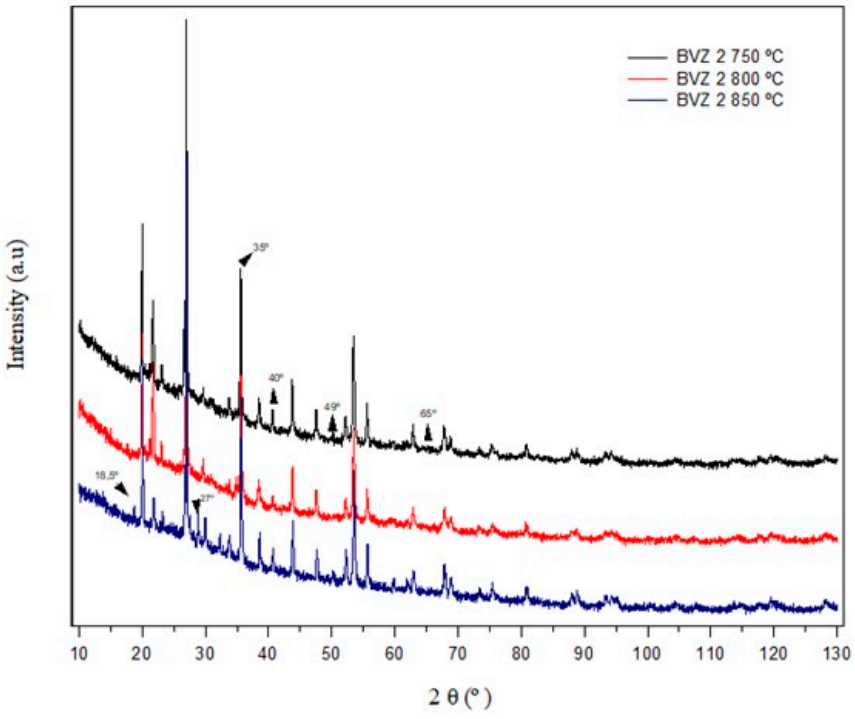

Figure 6. X-ray diffraction (XRD) patterns of BVZ2 glass-ceramics sintered at 750 °C, 800 °C, and 850 °C, showing the evolution of crystalline phases with increasing temperature.

In the sample sintered at 750 °C, zircon ($ZrSiO_4$, COD 96-900-2555) is predominant, accompanied by nepheline ($NaAlSiO_4$, COD 96-901-0305), cristobalite (SiO_2, COD 96-901-6226), and $AlPO_4$ (COD 96-155-0017). The higher fraction of zircon already at this temperature indicates that the increased Zr

 doi:10.20944/preprints202605.1253.v1

content in the composition favors the early crystallization of thermodynamically stable zirconium silicates, altering the devitrification pathway compared to BVZ1.

At 800 °C, a significant growth of the $AlPO_4$ phase (COD 96-155-0017) is observed, becoming comparable in intensity to zircon (COD 96-900-2557). This increase in the phosphate fraction indicates a greater participation of PO_4^{3-} groups in the structural reorganization of the glassy matrix, promoting the formation of P-O-Zr linkages. This structural reorganization represents an important step in the evolution of three-dimensional zirconium phosphate frameworks, often associated with the nucleation of NASICON-type phases in systems containing Na, Zr, and phosphates [27–29].

In the sample treated at 850 °C, the diffraction pattern becomes dominated by zircon (COD 96-500-0120), accompanied by $AlPO_4$ (COD 96-432-9331), nepheline (COD 96-100-8762), and cristobalite (COD 96-901-6226). Under this condition, an intensification of peaks is observed in the 27-33° (2θ) region as well as between 35-40° (2θ), angular ranges that coincide with characteristic reflections of sodium–zirconium phosphates with NASICON-type structure, such as $NaZr_2(PO_4)_3$.

Figure 7 illustrates the evolution of crystalline phases in the BVZ3 sample with increasing sintering temperature. At 750 °C, the most intense peaks correspond mainly to zircon ($ZrSiO_4$, COD 96-900-2555) and cristobalite (SiO_2, COD 96-901-7023), along with contributions from $AlPO_4$ in the form of α-moganite (COD 96-432-9331) and traces of nepheline ($NaAlSiO_4$, COD 96-900-9464). This set of phases indicates that, at this temperature, crystallization is still dominated by silicates, aluminosilicates, and aluminum phosphates formed through the structural reorganization of the glassy matrix.

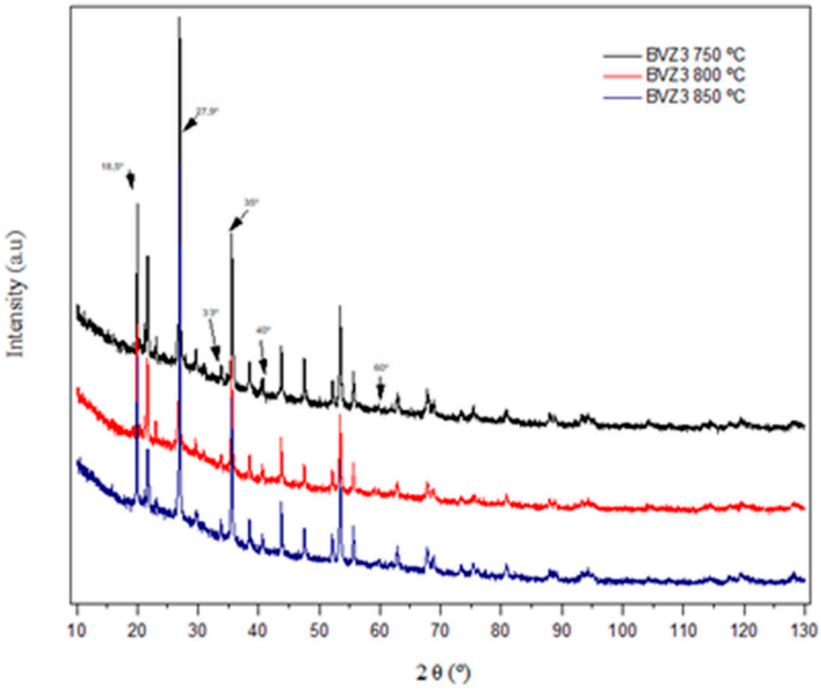

Figure 7. X-ray diffraction (XRD) patterns of BVZ3 glass-ceramics sintered at 750 °C, 800 °C, and 850 °C, showing the evolution of crystalline phases with increasing temperature.

With the temperature increased to 800 °C, a rise in the intensity of reflections associated with $AlPO_4$ (COD 96-155-0017) and zircon (COD 96-900-2560) is observed, accompanied by a relative reduction in nepheline contributions. At the same time, reflections in the approximate 27-33° (2θ) range become more evident, an angular region that coincides with characteristic peaks of sodium–zirconium phosphates with NASICON-type structure, such as $NaZr_2(PO_4)_3$ [27,28]. This behavior suggests that, as sintering progresses, species containing Na, Zr, and PO_4^{3-} groups play a greater role

 doi:10.20944/preprints202605.1253.v1

in structural reorganization, favoring the formation of more structurally ordered zirconium phosphate domains.

At 850 °C, the peaks become sharper and more intense, indicating crystal domain growth and increased structural order. Zircon (COD 96-500-0120) remains the major phase, while alumino-phosphate and sodium silicate phases show a lower relative contribution. The persistence and improved definition of reflections in the 27-33° (2θ) region reinforce the possibility of the formation of domains structurally compatible with the three-dimensional NASICON-type framework.

Thus, for the BVZ3 composition, the presence of a NASICON-type phase can be considered probable in minor amounts, favored by the increase in sintering temperature and the coexistence of Na, Zr, and phosphate groups within the glassy matrix.

Overall, the progressive evolution from BVZ1 to BVZ3 indicates that increasing the availability of Zr and phosphates promotes the structural conditions necessary for the nucleation of NASICON-type domains, although these remain secondary phases masked by the predominant silicate and zircon phases.

3.2.3. Thermal Behavior and Crystallization of Glass-Ceramics (DTA)

Figure 8 shows the Differential Thermal Analysis (DTA) curves of the BVZ1 (a), BVZ2 (b), and BVZ3 (c) glass-ceramics sintered at 750 °C, 800 °C, and 850 °C, obtained under a heating rate of 10 °C·min^{-1} in a N_2 atmosphere. The characteristic thermal parameters, glass transition temperature (Tg), crystallization temperature (Tx), and partial melting temperature (Tm), are summarized in Table 6.

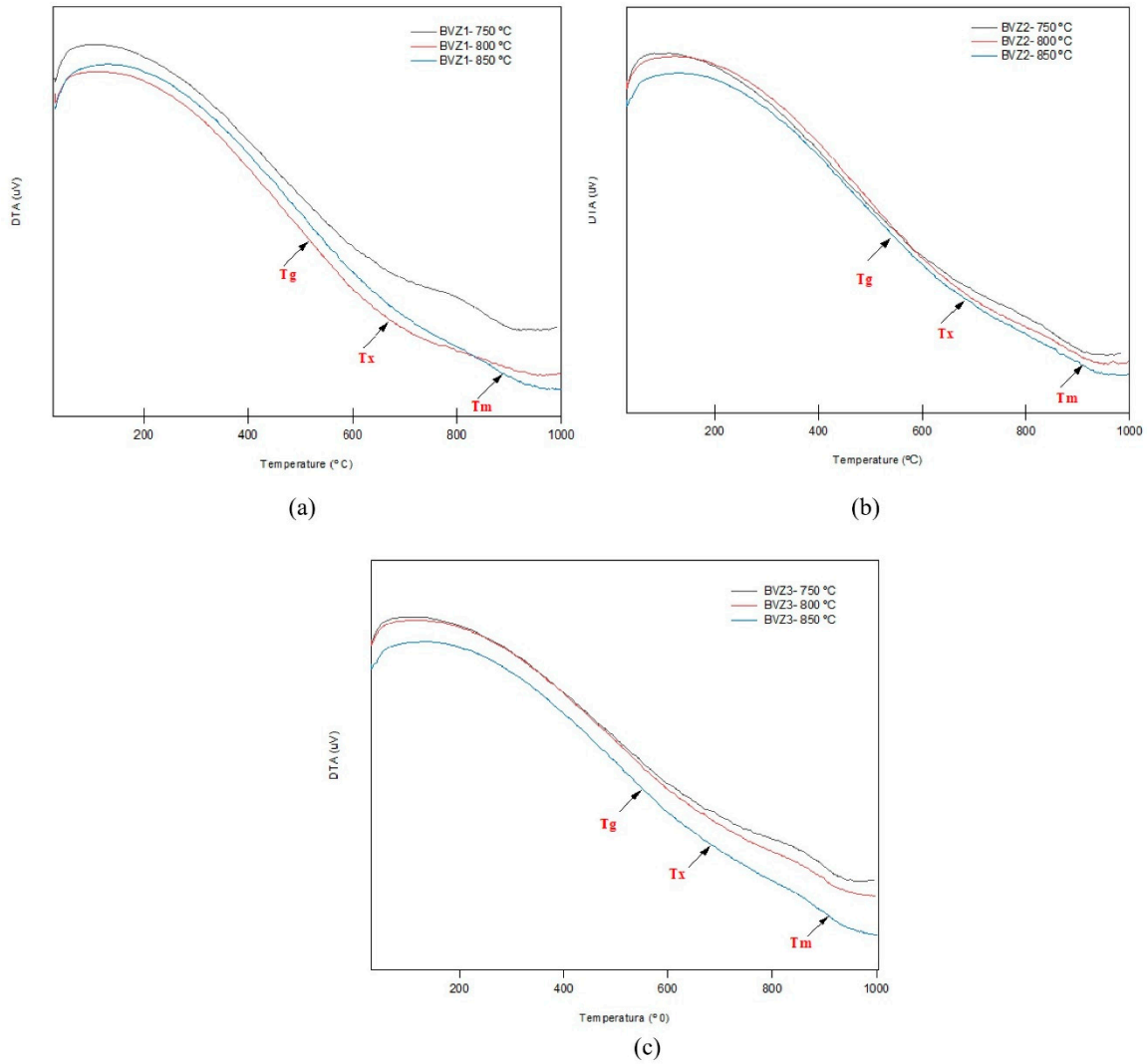

 doi:10.20944/preprints202605.1253.v1

Figure 8. DTA curves of BVZ1 (**a**), BVZ2 (**b**), and BVZ3 (**c**) glass-ceramics sintered at 750, 800, and 850 °C, obtained at a heating rate of 10 °C·min^{-1} under a N_2 atmosphere.

Table 6. Characteristic temperatures of glass-ceramics.

Samples	Sintering Temperature (°C)	Tg (°C)	Tx (°C)	Tm (°C)
BVZ 1	750	438	599	930
	800	420	603	802
	850	440	548	868
BVZ 2	750	435	556	848
	800	432	604	850
	850	420	621	849
BVZ 3	750	422	621	964
	800	372	557	904
	850	413	590	897

The glass transition temperature (Tg), identified as an inflection in the baseline, shifts to higher values with increasing sintering temperature. This behavior indicates increased rigidity of the residual glassy phase, associated with reduced structural mobility and enhanced network polymerization after partial crystallization, a phenomenon typical of glass systems undergoing structural stabilization [30,31].

The subsequent exothermic event (Tx), visible in the curves of Figure 8a-c, is related to the crystallization of the remaining glassy phase. The progressive decrease in the intensity of this peak in samples treated at higher temperatures indicates that crystallization had already advanced during sintering, resulting in a smaller amorphous fraction available for further thermal transformation. This behavior confirms the typical progressive microstructural evolution of glass-ceramics at advanced crystallization stages [31].

A slight shift of Tx toward higher temperatures is also observed in samples sintered at 850 °C, suggesting increased thermal stability of the partially crystallized microstructure. This effect is associated with the presence of previously formed crystalline phases, which reduce diffusional mobility and increase the energy required for further crystal growth [30].

At higher temperatures, the broad endothermic trend observed in the curves is related to structural relaxation and viscous flow of the residual glassy phase and may also involve partial reorganization of crystalline phases. Differences in this behavior among BVZ1, BVZ2, and BVZ3 reflect compositional variations that influence the viscosity of the residual glass and the thermal stability of the formed phases [30].

Comparatively, BVZ3 (Figure 8c) shows a lower crystallization peak intensity and a greater Tg shift, indicating a higher degree of prior crystallization and enhanced structural stabilization. BVZ1 (Figure 8a) retains a larger residual glass fraction, while BVZ2 (Figure 8b) exhibits intermediate behavior. Overall, the DTA results demonstrate that increasing the sintering temperature promotes greater structural ordering, reduction of the amorphous fraction, and improved thermal stability of the BVZ glass-ceramics.7

3.2.4. Surface Microstructure and Porosity Evolution

Figure 9 shows optical micrographs obtained from the surface of BVZ1, BVZ2, and BVZ3 glass-ceramic foams sintered at 750 °C, 800 °C, and 850 °C. In general, increasing both the glass waste

 doi:10.20944/preprints202605.1253.v1

content and the sintering temperature led to a reduction in porosity. This behavior is associated with enhanced viscous flow of the glassy phase and progressive densification during liquid-phase sintering [23,30].

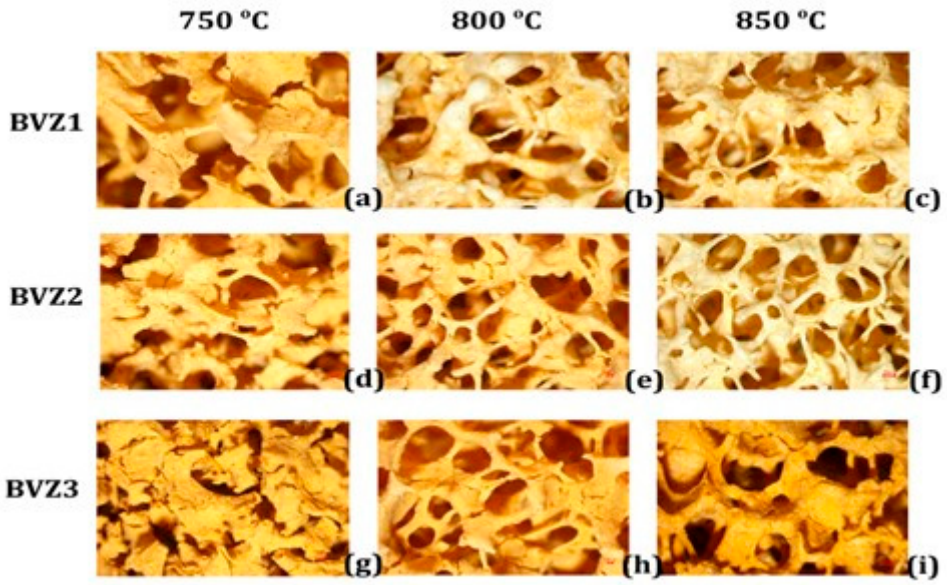

Figure 9. Optical micrographs (500**µ**m) acquired from the surface of the BVZs foams. (**a**) BVZ1-750 °C, (**b**) BVZ1-800 °C, (**c**) BVZ1-850 °C, (**d**) BVZ2-750 °C, (**e**) BVZ2-800 °C, (**f**) BVZ2-850 °C, (**g**) BVZ3-750 °C, (**h**) BVZ3-800 °C e (**i**) BVZ3-850 °C.

As expected, for a given glass-ceramic foam composition, increasing the temperature increased the amount of liquid phase formed during sintering. This liquid phase penetrated the strut channels within the foams, sealing pores and consequently increasing the bulk density. Such pore closure is typical of glass-based foams subjected to higher thermal treatments, where reduced viscosity promotes mass transport and structural consolidation [23].

At all investigated temperatures, pore closure became more pronounced as the glass waste content increased. This trend indicates that higher amounts of low-viscosity glass favor the formation of a continuous liquid network during sintering, enhancing particle bonding and reducing open porosity.

3.2.5. Compressive Strength of Glass-Ceramic Foams

The results of uniaxial compressive strength for the BVZ glass-ceramic system are presented in Table 7 and Figure 10. Only compositions that exhibited sufficient structural integrity for handling were selected for testing, a criterion met by samples sintered at 800 °C and 850 °C. Increasing the sintering temperature to 850 °C, combined with a higher glass waste content in the BVZ-1 formulation, promoted the formation of a larger amount of liquid phase.

 doi:10.20944/preprints202605.1253.v1

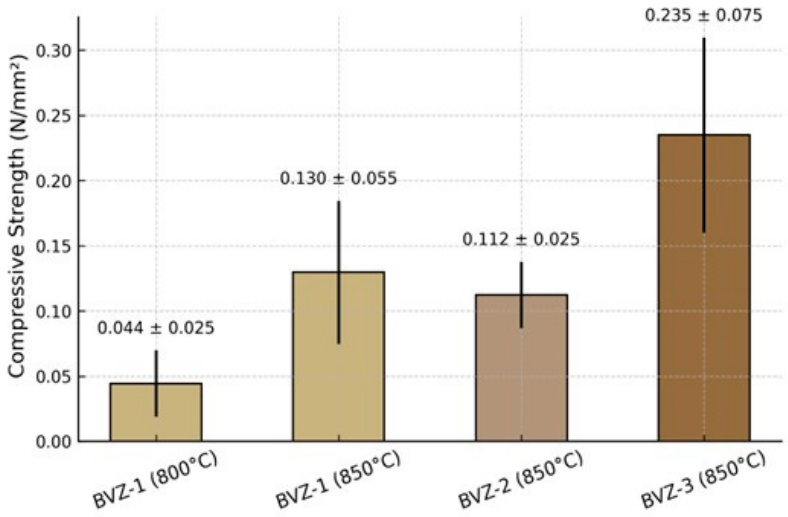

Figure 10. Compressive strength of BVZ glass-ceramics at 800 °C and 850 °C (mean ± SD).

Table 7. Compressive strength of BVZ glass-ceramics heat-treated at 800 °C and 850 °C (mean ± SD).

Glas-Ceramics Temperature °C	Compressive Strength (N/mm²)	Standard Deviation (N/mm²)
BVZ1 - 800 °C	0.044	0.025
BVZ1 - 850 °C	0.130	0.055
BVZ2 - 850 °C	0.112	0.025
BVZ3 - 850 °C	0.235	0.075

This phenomenon led to the consolidation of a continuous glassy matrix acting as a binding phase between the refractory zirconia and bentonite particles. In addition, the granulometric synergy between the precursors allowed the glassy phase to coat the particles, reducing residual porosity and improving mechanical stress distribution more effectively. This behavior is consistent with the findings of Owoeye et al. [32], who reported an inverse relationship between porosity and strength, indicating that the mechanical integrity achieved is compatible with the operational requirements for use as electrodes.

5. Conclusions

Glass-ceramic foams were successfully produced using approximately 85 wt% soda-lime glass waste and zirconia-containing residues. Variations in color and microstructure were influenced by both composition and sintering temperature. Increasing the glass waste content and raising the sintering temperature to 850 °C promoted enhanced densification, as evidenced by reduced porosity observed in the micrographs.

X-ray diffraction analysis indicated that crystallization in the BVZ system is predominantly governed by phases of silicates and aluminosilicates, especially nepheline ($NaAlSiO_4$) and zircon ($ZrSiO_4$), whose crystallinity increased with temperature. In addition, tetragonal zirconia (t-ZrO_2) was identified, and minor domains structurally compatible with NASICON-type phases ($NaZr_2(PO_4)_3$) were suggested, particularly in BVZ2 and BVZ3 sintered at 850 °C, although these remain secondary compared to the dominant silicate and zircon phases.

The mechanical behavior of the glass-ceramic foams demonstrated compressive strength sufficient to withstand handling and assembly stresses associated with electrochemical cell components. The reduced fragility observed at higher sintering temperatures further supports their structural integrity and potential for scalable processing.

 doi:10.20944/preprints202605.1253.v1

Overall, the combined structural, microstructural, and mechanical results indicate that the controlled devitrification of glass waste–based compositions can yield porous glass-ceramics with promising characteristics for structural and functional applications.

Author Contributions: Conceptualization, Edson de Oliveira Costa and Crislene Rodrigues da Silva Morais; methodology, Edson de Oliveira Costa, Maria Aparecida Ribeiro Bonifácio and Adriana de Jesus Santos; software, Cochian Pereira dos Santos; validation, José Carlos Martins de Almeida, Eliane Bezerra Cavalcanti and Crislene Rodrigues da Silva Morais; formal analysis, Edson de Oliveira Costa, Cochian Pereira dos Santos and Valdenia Porto Medeiros; investigation, Edson de Oliveira Costa, Maria Aparecida Ribeiro Bonifácio and Adriana de Jesus Santos; resources, José Carlos Martins de Almeida, Eliane Bezerra Cavalcanti and Crislene Rodrigues da Silva Morais; data curation, Edson de Oliveira Costa and Cochian Pereira dos Santos; writing—original draft preparation, Edson de Oliveira Costa; writing—review and editing, Crislene Rodrigues da Silva Morais, José Carlos Martins de Almeida and Eliane Bezerra Cavalcanti; visualization, Edson de Oliveira Costa and Cochian Pereira dos Santos; supervision, Crislene Rodrigues da Silva Morais and Eliane Bezerra Cavalcanti; project administration, Crislene Rodrigues da Silva Morais; funding acquisition, José Carlos Martins de Almeida and Crislene Rodrigues da Silva Morais. All authors have read and agreed to the published version of the manuscript.

Acknowledgments: The authors acknowledge the Materials and Glass Synthesis Laboratory (LASMAV/UAEMa/UFCG) and the Thermal Analysis Laboratory (LABTERM/UAEMa/UFCG) for providing the infrastructure for the synthesis of the glass-ceramics and thermal analyses. The authors also thank the University of Aveiro (DEMaC/UAveiro) for the X-ray diffraction and mechanical strength testing. Morais, C.R.S. acknowledges the National Council for Scientific and Technological Development (CNPq) for the award of a postdoctoral fellowship. CAPES Process Number: 88887.828542/2023-00.

Conflicts of Interest: Declaration of competing interest. The authors declare that they have no known competing financial interests or personal relationships that could have appeared to influence the work reported in this paper.

Abbreviations

BVZ	Bottle glass waste–zirconia residue–bentonite

References

1. F.P. Costa, C.R.S. Morais, A.M. Rodrigues, Sustainable glass-ceramic foams manufactured from waste glass bottles and bentonite, *Ceram. Int.* 46 (2020) 17957–17961.
2. F.P. Costa, C.R.S. Morais, H.C. Pinto, A.M. Rodrigues, Microstructure and physico-mechanical properties of Al_2O_3-doped sustainable glass-ceramic foams, *Mater. Chem. Phys.* 256 (2020) 123612.
3. C.R. Bowen, T. Thomas, Macro-porous Ti_2AlC MAX-phase ceramics by the foam replication method, *Ceram. Int.* 41 (2015) 12178–12185.
4. L.P. Wang, P.W. Tseng, K.J. Huang, Y.J. Chen, Foam glass production from waste bottle glass using silicon cutting waste as foaming agent, *Constr. Build. Mater.* 383 (2023) 131344.
5. K. Yu, J. Xie, C. Cai, et al., Sustainable fabrication of high-strength and thermally conductive porous SiC ceramics from recycled waste glass, *Ceram. Int.* (2025).
6. W. He, Y. Wu, B. Dong, et al., Processing and applications of glass-ceramics: A comparative review, *Ceram. Int.* (2026).
7. S.M. Salman, S.N. Salama, E.A. Mahdy, Crystallization and thermo-mechanical properties of Li_2O–ZnO–CaO–SiO_2 glass-ceramics, *Process. Appl. Ceram.* 9 (2015) 215–223.
8. J. Zhou, J. Lu, C. Liu, L. Chen, Preparation and properties of uniformly porous glass-ceramics, *Ceram. Int.* (2024).
9. H. Gao, et al., The influence of different foaming agents on foam ceramics, *Crystals* 15 (2025) 606.
10. R.C.B. Albuquerque, et al., Ceramic foams added with flat glass waste by the replica method, *Rev. Eletrôn. Mater. Process.* 14 (2019) 54–59.

 doi:10.20944/preprints202605.1253.v1

11. S. Seidel, M. Dittmer, W. Wisniewski, et al., Effect of ZrO_2 concentration on crystallization behavior, *J. Mater. Sci.* 52 (2017) 1955–1968.
12. C. Oliveira, M. Rocha, A. Silva, L. Bertolino, Characterization of bentonitic clays from Paraíba, *Cerâmica* 62 (2016) 272–277.
13. R.F. Silva, X-ray diffraction as a technique for crystalline structure investigation, *Rev. Processos Quím.* 14 (2020) 73–82.
14. S. Taoussi, A. Ouaha, M. Naji, et al., Zn-doped NASICON-based glass-ceramic with superior Li-conductivity, *Acta Mater.* (2025).
15. J.F. Ortiz-Mosquera, A.M. Nieto-Muñoz, A.C. Rodrigues, Glass-ceramics from NASICON series, *J. Non-Cryst. Solids* 513 (2019) 36–43.
16. J. Liu, Q. Wang, Z. Zhang, et al., Crystallization behavior of Li_2O–Al_2O_3–SiO_2 glasses, *J. Non-Cryst. Solids* 576 (2022) 121226.
17. W. Höland, G.H. Beall, *Glass-Ceramic Materials*, 2nd ed., Wiley, 2019.
18. O. Jing, Y. Peng, W. Zhou, et al., Oxygen vacancies in nanocrystalline ZrO_2, *Nanomaterials* 14 (2024).
19. M. Marlina, et al., Preparation and characterization of zirconia nanomaterials, *Atom Indones.* 43 (2017) 1–6.
20. D. Radulović, et al., Comprehensive characterization of natural bentonite clay, *Sci. Sinter.* (2025).
21. C. Souto, et al., Rheological performance of bentonitic clays, *Rev. Princípios* (2020).
22. J. Cuevas, et al., Quantitative XRD analysis of bentonite powder, *Minerals* 12 (2022) 772.
23. Ortiz, A. L., Rodrigues, C. S., Guiberteau, F., & Zhang, Y. (2021). Microstructural development during crystallization firing of a dental-grade nanostructured lithia-zirconia glass-ceramic. Journal of the European Ceramic Society, 41(11), 5728-5739.
24. J. Liu, et al., Crystallization behavior of Li_2O-Al_2O_3-SiO_2 glasses, *J. Non-Cryst. Solids* 576 (2022).
25. M. Hammi, et al., Glass-to-crystal transformations: XRD investigation, *Materials* 16 (2023).
26. R.F. Silva, XRD technique for crystalline structure investigation, *Rev. Processos Quím.* 14 (2020).
27. H.P. Hong, Crystal chemistry in the $Na_{1+x}Zr_2Si_xP_{3-x}O_{12}$ system, *Mater. Res. Bull.* 11 (1976) 173–182.
28. J.B. Goodenough, H.Y.P. Hong, J.A. Kafalas, Fast Na^+-ion transport in skeleton structures, *Mater. Res. Bull.* 11 (1976) 203–220.
29. B. Zarabian, B.E. Yekta, S. Banijamali, Crystallization behavior of NASICON-type glass-ceramics, *Synth. Sinter.* 3 (2023) 14–19.
30. J.E. Shelby, *Introduction to Glass Science and Technology*, Royal Society of Chemistry, 2020.
31. E.D. Zanotto, J.C. Mauro, The glassy state of matter, *J. Non-Cryst. Solids* 471 (2017) 490–495.
32. S.S. Owoeye, et al., Preparation and characterization of foam glass from waste container glasses, *Ceram. Int.* 46 (2020) 11770–11775.
33. V.D.S. Porto, *Development of cellular porous ceramics using waste glass and fluorescent lamp residues in its composition*, PhD Thesis, Federal University of Campina Grande (UFCG), Campina Grande, Brazil, 2016.